RECENT FREE-FLIGHT BOUNDARY-SURFACE AERODYNAMIC NOISE MEASUREMENTS

By I. E. Garrick, D. A. Hilton, and H. H. Hubbard

NASA Langley Research Center
Langley Station, Hampton, Va., U.S.A.

Presented at a Specialists' Meeting
on "The Mechanism of Noise Generation in Turbulent Flow"
Under the Sponsorship of the Fluid Dynamics Panel of the Advisory
Group for Aeronautical Research and Development

Rhode-Saint-Genese, Belgium
April 1-5, 1963

NATIONAL AERONAUTICS AND
SPACE ADMINISTRATION
WASHINGTON

RECENT FREE-FLIGHT BOUNDARY-SURFACE AERODYNAMIC NOISE MEASUREMENTS

by

I. E. Garrick*, D. A. Hilton**, and H. H. Hubbard***

SUMMARY

This paper contains a review of recent measurements of fluctuating pressures due to airflow over surfaces. Included are data from aircraft, missiles, and space vehicles for wide ranges of dynamic pressure and Reynolds number for both subsonic and supersonic speeds. Several sources of turbulence that result in severe vehicle loads and vibration environments are discussed, including results for surface flow conditions of developed boundary-layer turbulent flows and others for buffeting types of flow. Also included is brief mention of recent information on the large scale turbulence characteristics of the atmosphere.

Correlations based on free-stream dynamic pressure are presented for a variety of flow conditions, including flow separation and possible shock wave interactions. These results indicate a relatively weak dependence of the surface pressure coefficient on Mach number, but the coefficient may vary markedly depending on the local flow conditions.

---

*Chief, Dynamic Loads Division
**Aerospace Engineer
***Head, Acoustics Branch

L-3361

A speed effect is noted as a general result of these tests; in particular, the spectra at the higher Mach numbers contain relatively more high frequency noise and relatively less low frequency noise than spectra measured at low speeds.

INTRODUCTION

Any vehicle which passes through a fluid medium or atmosphere has impinging on its surface fluctuating pressures associated with the flow. The character of these pressure disturbances may be a function of the vehicle configuration including its surface conditions, the operating conditions or trajectories of the vehicle, and to some extent the atmosphere itself. Although the subject is old, interest has been intensified in recent years because aerodynamically induced disturbances are inherently more important in the design of high speed vehicles such as advanced aircraft, missiles, and space vehicles. For such vehicles, aerodynamic noise is significant from the standpoint of vehicle loads and vibration environment and may result in excitation of modes of the structure, cause sensitive equipment to malfunction, or interfere with normal duty activity of vehicle occupants or with the comfort of passengers.

The sources of the unsteady pressures may reside in the relatively large scale turbulence characteristics of the atmosphere itself or in

intermediate scale turbulence associated with various kinds of buffeting flows, or in the small scale turbulence of boundary-layer flows.

In the study of these phenomena and the problems that arise from them, it is found that there occur features in common, sometimes phenomena merge, and often similar random process techniques may be employed analytically and experimentally.

There have been relatively few in-flight measurements of the fluctuating aerodynamic pressures at the boundary surfaces of high speed vehicles. Although such flight measurements often do not reveal significant details of the generation of the "noise", they do point to the environmental problems of significance for investigation relative to design loads, to vehicle operation, and to the comfort of occupants. Flight information on unsteady pressures for launch vehicles is particularly scarce or practically nonexistent; accordingly, a main objective of this paper is to present certain recent data for flight Mach numbers up to about 4 for the Scout vehicle. As a further objective, we will briefly review recently published aerodynamic-noise flight data on aircraft and similar data obtained in connection with the Mercury project. As a third objective, it has seemed appropriate because of its relevance to turbulence in general, to include in the paper, actually in the initial section, brief discussion of several recent contributions to the grosser scale "noise" problems of flight which relate to atmospheric turbulence and to buffet.

It may thus be of interest for purposes of orientation to examine

in figure 1 the sources of vibration and turbulence referred to and their frequency ranges of significance. Contributions to these items as already indicated will be taken up in turn in the following sections.

RECENT INFORMATION ON THE SPECTRUM AND SCALE OF ATMOSPHERIC TURBULENCE

Airplane flight in atmospheric turbulence.- During the past decade interest has attached itself to the description of atmospheric turbulence as a continuous (rather than discrete) process and to the use of atmospheric spectra in the analysis of gusts and dynamic response of aircraft. During 1959 a flight investigation was made on the spectrum of turbulence in cumulus clouds around 15,000 feet altitude near Langley Field, Virginia. In 1960 and again in 1961, an investigation of airplane response and of the spectrum of turbulence was made at high subsonic and at supersonic flight speeds for squall lines and thunderstorms in midwestern United States in a cooperative severe storms project involving NASA, USAF, and the U. S. Weather Bureau. A significant account of several phases of these investigations was given in a report to AGARD in July 1962 prepared by J. C. Houbolt, Roy Steiner, and K. G. Pratt (ref. 1). For the present purpose, we wish to present and discuss only a selection of a few high spots on the spectrum results and on the determination of the scale of turbulence. As will be seen, these items tie in closely with current theoretical models of

isotropic turbulence.

The time history of a component of gust velocity (vertical, lateral, or longitudinal) is obtained from flight measurement of local angle of attack by means of flow vanes or differential pressure probes on a boom ahead of the airplane with due account taken for airplane motion. The time history is analyzed to determine the autocorrelation function and the power spectrum by numerical techniques involving some 2,000 readings per record (100 seconds).

A typical set of spectra is shown in figure 2 for 3 sets of weather conditions: clear air turbulence, cumulus clouds, and thunderstorms (traversed at 40,000 feet altitude). The similarity in the slopes of the spectra is apparent. The variation in intensity is indicated by the relative heights as well as by the value of σ_1 , the root-mean-square gust velocity, a truncated value obtained from area under the measured curves. (It is of interest to mention that wherever the vertical, lateral, and longitudinal components were measured, they corresponded reasonably with isotropic assumptions. Also, the various traverses showed that even the thunderstorm's turbulence corresponded to reasonably stationary processes over time intervals greater than the duration of a single flight recording.)

Two types of analytical representation (as indicated by the equations in figure 3) were employed to fit and compare the correlations and the spectral shapes. Case I is deduced from an expression for three-dimensional isotropic turbulence given by von Karman (ref. 2)

using G. I. Taylor's one-dimensional form of the spectrum. Von Karman's expression, it may be recalled, was chosen by him to fit the low frequency range behavior of the power spectra as proportional to $(\text{freq.})^4$ (L. Loitsiansky; C. C. Lin) and to fit a high frequency power law $(\text{freq.})^{-5/3}$ (Kolmogoroff, and others). Case II, on the other hand, is a frequently employed representation based on exponential type correlation for turbulent diffusion and yielding a high frequency range proportionality for the power spectra as $(\text{freq.})^{-2}$.

Only the first type, the one which fits the results best, will be exhibited; the family of analytical power spectral curves is shown in figure 4. The family depends on a scale parameter L which can be determined from either a given correlation curve or a given power spectral curve, and is a measure of the size of the main physical process in the turbulent diffusion.

A measured spectrum and a fitted curve for $L = 5600$ ft are indicated in figure 5. The basic parameter σ, the root-mean-square gust velocity, which is involved is obtained from the measured auto-correlation function. The evaluation of L, as well as the fit of the data with case I type curves, that was discussed in reference 1 is a matter of considerable interest. The value of L can be found from the numerically determined autocorrelation or power spectrum curve corresponding to the measured data on the basis of the chosen analytical representation. Interestingly enough, although the basic definitions of L may require integration from 0 to ∞, it develops

that one need employ only integration over the most reliable range defined by the data. As is indicated in the table in figure 6, a comparison of the value of L was more consistent with the fitted curves for both the power spectrum and the correlation curve for case I than for case II and shows the value of L for the thunderstorm turbulence to be of the order of 5,000 feet. Of special interest is the fact that while σ_1, the truncated root-mean-square velocity, is 13.38 ft/sec, the value σ for the complete curve in figure 5 is 32.33 ft/sec.

Vertical flight of boosters.- Although the gust loads and dynamic response problems of aircraft may be put on a rational design basis by spectral methods for continuous turbulence, no such methods have yet proved useful in regard to vertical flight for boosters. It may be of interest to briefly discuss the need for additional information on ground winds and of wind shear characteristics in this connection. As figure 7 indicates, on the launch pad and during prelaunch operations the vehicle is subjected to steady and unsteady horizontal winds which vary with time and height above terrain. Interestingly enough the unsteady part in the neighborhood of the ground has been shown to have a scale proportional more or less to the altitude and to possess many of the characteristics of isotropic turbulence. The deflections produced by both steady and unsteady ground winds bring about problems in structural strength, guidance alinement, and flight instrumentation checkouts.

Wind shear characteristics affect loads and guidance during the launching phase. Figure 8 shows horizontal components of wind as

measured by a smoke trail technique. Details not ordinarily found in balloon measurements show up that indicate many reversals in the unsteady wind structure. Figure 9 shows some measurements for which the magnitudes of the winds were particularly large.

A design envelop for a large launch vehicle is indicated in figure 10 giving the design structural bending moment against vehicle station. It may be noted that for this particular case the bending moment for the bottom 25% of the structure is determined by ground winds criteria while that of the remaining structure is based on wind-shear criteria. The unsteady or turbulent part of the wind contributes only a fraction (about 1/4) of the total bending moment and depends on the assumed elastic vehicle characteristics.

REMARKS ON PRESSURE FLUCTUATIONS IN BUFFETING

Large pressure fluctuations may be experienced by a flight vehicle in buffeting flows associated with boundary-layer separation. Because the values of these pressures may exceed boundary-layer noise levels by more than an order of magnitude, it is appropriate to include a few figures and remarks (refs. 3 and 4).

Figure 11 indicates some of the various types of buffeting flows that have been identified on launch vehicles during transonic flows. Sketch (a) refers to buffet created by boundary-layer separation following a strong shock. Sketch (b) refers to an unstable shock

situation wherein the flow may alternate from subsonic to supersonic with the shock wave jumping back and forth and with flow separation and reattachment occurring. Sketch (c) refers to buffeting arising from impingement or proximity of the wake of a forward component or projection of an aft component.

Figure 12 shows two types of power spectrums which have been obtained. For the one corresponding to sketch (a) the power is concentrated in the lower frequency range, while for the other corresponding to sketch (c) the power is distributed over a wide range of frequencies resulting in a white type of noise. (The power spectrum corresponding to the buffeting indicated in sketch (b) is also contained in the low frequency range, a range even lower than for sketch (a)). The low frequency type will excite, for example, the bending modes of the whole vehicle, while the white noise type will excite local structure such as panels or attachments. The low frequency buffet corresponds to excitation by large size vortices and the aerodynamic input is three-dimensional in nature; consequently it is difficult to represent this input analytically. The wake type buffet tends to be smaller scale and more isotropic in nature. Some investigation of the feasibility of scaling a vehicle for study of the buffeting phenomena in a wind tunnel has been made. With moderate care in the scaling, providing a reasonable Reynolds number for the flow and a suitable elastic model are employed, it appears feasible to reproduce the phenomena and to predict the loads to be experienced on the full scale

vehicle with engineering accuracy.

It may be of interest to present an estimate of the external acoustic environment to be expected for a manned lunar vehicle during launch. Some of the data were based on scaled model tests, while others were based on flight data to be discussed at a later point. The estimated noise levels are made for a region of the vehicle where the manned compartment might be located. Figure 13, taken from reference 5, shows noise levels from engines and from buffeting or aerodynamic sources as a function of time. Engine noise levels are based on measured data obtained for Saturn static firings and Atlas launching tests. The highest engine noise levels are indicated at liftoff because of flow turning and ground reflections. There is a decrease in engine noise levels after the vehicle leaves the ground because of beneficial effects of the forward motion, the receding of the ground, and the straightening of the flow. Aerodynamic noise levels begin to predominate as the dynamic pressure increases. Levels shown are not average values, but the worst to be expected regardless of location. (Full curve is based on model data, dashed curve is based on extrapolation using a somewhat different configuration.) The lower solid curve of figure 13 represents a minimum expected noise level as based on results for attached turbulent boundary layers.

AVAILABLE FREE FLIGHT DATA

The free flight conditions for which boundary surface noise data are available can be summarized with the aid of figures 14 and 15. In figure 14 are plotted the ranges of dynamic pressure associated with the operations of three types of test vehicles as a function of Mach number. It can be seen that data are available for fighter type aircraft for Mach numbers up to 2 and for dynamic pressures up to approximately 1100 lbs/sq ft (refs. 6-9). For subsonic transport and bomber aircraft, data are available in the Mach number range of about .4 to .8 and for dynamic pressures up to about 600 lbs/sq ft (refs. 10-12). The available information for launch vehicles has come mainly from the Mercury development program for which data have been obtained up to about Mach number 5 and for dynamic pressures up to about 3,000 lbs/sq ft (ref. 13). The dynamic pressures of direct interest for launch vehicles vary widely; generally the highest values are associated with solid fuel vehicles, whereas the lower values are associated with liquid fuel vehicles.

Likewise, the ranges of Reynolds numbers for the available data are indicated in figure 15. It can be seen from this figure that the Reynolds numbers (based on distance from the leading edge to the measuring station) attained in the fighter aircraft tests were limited to about 30 million, whereas the bomber and launch vehicle data extend to roughly 200 and 400 million respectively. To summarize the

information of figures 14 and 15, it can be seen that data obtained with the aid of fighter aircraft have covered a substantial Mach number and dynamic pressure range but have been generally limited to relatively low Reynolds numbers. In the case of data obtained with bomber and subsonic transport aircraft, the Reynolds numbers were substantially higher but the Mach number and dynamic pressure ranges were rather limited.

In the present section of the paper, an attempt will be made to briefly review the available free flight data from aircraft and launch vehicles. Some data measured inside of the vehicle as well as surface pressure data will be included.

In order to indicate the manner in which aerodynamic noise in the interior compartments varies as a function of Mach number, data from several aircraft are plotted in figure 16. The basic data of this figure were taken from reference 14, and the more recent results from B-47, D-558, and F-102 studies have been added. It can be seen that the noise levels increase with Mach number at about the same rate for all the aircraft even though they obviously may differ widely in shape, size, and method of construction. From the slopes of the curves it can be deduced that on the average, the inside noise pressures increase as approximately the 2.5 power of the Mach number. The differences in levels of the noise at a given Mach number can partly be accounted for by differences in the altitudes of operation, the outside contours and surface conditions of the vehicle, and the transmission characteristics

of the vehicle wall. An attempt has been made to account for differences in altitude and sound transmission in reference 15, and it was found that the scatter of similar data from comparable types of aircraft was reduced to about $\pm$ 4 db.

An attempt is made in figure 17 to summarize the surface pressure data measured on several fighter and bomber aircraft, and these are compared with channel flow data at high Reynolds numbers obtained by Willmarth in reference 16. Surface pressure levels are plotted as a function of dynamic pressure. All data were recorded in the altitude range 20,000 to 26,000 feet and for subsonic Mach numbers, with the exception of the F-104 data which extend to Mach 1.6. It can be seen that the surface pressure levels measured for the B-47, the B-57 fuselage, and the T-33 fuselage seem to group together just below the channel flow data and follow roughly the same trend as a function of dynamic pressure. On the other hand, the measurements for the F-104 nose cone and the T-33 wing are considerably lower in magnitude. In these latter two cases, the transducers may have been located in regions where the flow was not fully developed, and furthermore the transducer size may be large relative to the boundary-layer thickness.

Further information relative to the physical characteristics of the fluctuating pressures of figure 17 are indicated by the frequency spectra of figure 18. Octave band spectra are shown in this figure corresponding to the measuring conditions of figure 17. The fuselage spectra are seen to have a broad peak in the audible frequency range.

The nose cone and wing data, on the other hand, suggest a possible peak in the ultrasonic frequency range. This result is probably due at least in part to the fact that the Reynolds numbers represented by those latter measuring conditions are relatively lower.

In order to provide free flight data in the Mach number, Reynolds number, and dynamic pressure ranges of direct interest for various launch vehicles and also for the supersonic transport, it has been necessary to make use of launch vehicles. Some of these launch vehicle data, which were obtained during the Mercury development program, are summarized herein. Of particular interest are comparable external and internal sound pressure level time histories obtained for one of the vehicles of the Mercury program as presented in figure 19. This was a suborbital flight for which data were obtained during the exit phase flight. The main events of the flight, such as the liftoff, maximum dynamic pressure, and firing of the escape system rockets, are indicated in the figure. The first peak of the external time history trace occurs as a result of the firing of the rocket booster engine. The subsequent broad peak is believed to be due to noise of aerodynamic origin, and this is followed by a noise peak due to the firing of the escape system rocket engines.

It may be noted that the shapes of the external and internal time history curves are markedly different. In particular, it can be seen that the broad peak due to noise of aerodynamic origin occurs at an earlier time in the external time history trace than it does in the

internal time history trace. It is believed that the pressures measured at an external point on the surface (see sketch), as in figure 19(a), are closely related to the local flow conditions at that point and thus probably vary as a function of time since the Mach number, dynamic pressure, and the altitude are varying. The time history trace of the internal noise level, on the other hand, represents an integration of the noise events over a sizeable area of the spacecraft surface, and within this area there may be rather large variations in the local flow conditions.

A distinguishing characteristic of the external surface pressure data is the presence of relatively intense, low frequency components for the low Mach number range of the flight. This phenomenon is illustrated in figure 20 by the one-third octave band spectra which were obtained near Mach 1 and also near Mach 2, which corresponds approximately to the maximum dynamic pressure condition of the flight. Data are presented for point A, which is on the surface of the manned capsule, and for point B, which is on the surface of the booster adapter section of the vehicle. It can be seen from a comparison of the data at point A that spectra differ for the two different Mach numbers. The Mach 1.0 spectrum peaks broadly below 200 cps, whereas the Mach 2.0 spectrum peaks at higher frequencies. The data measured at point B cover a narrower frequency range but indicate higher levels at corresponding frequencies, and the shapes of the curves are somewhat similar to those at point A. Although the local flow conditions were not measured during

any of these flights, regions of intense buffeting along the spacecraft surface have been indicated in wind tunnel model studies.

The external surface pressure data measured for this same vehicle are shown in figure 21 where the ratio of external surface pressure to dynamic pressure is presented as a function of flight Mach number. Also shown in the figure is a dashed line representing the maximum values that would have been estimated on the basis of wind tunnel studies of flow over smooth surfaces (ref. 16) and the low speed flight data of figure 16. The surface pressure data for this vehicle are noted to be higher at low Mach numbers than the maximum pressure ratio values that would have been predicted for a vehicle with smooth aerodynamic surfaces. A distinguishing characteristic of the external surface pressures in the region of the highest measured values of figure 21 is the existence of large amplitude, low frequency disturbances of the type suggested in the Mach number 1.0 spectra of figure 20. The presence of these low frequency disturbances is believed, in this case, to result mainly from the presence of the aerodynamic spoiler shown schematically in the sketch of figure 21 and which was added to increase the aerodynamic stability of the basic configuration.

This effect of external contouring is further illustrated with the aid of the data of figure 22 which were measured inside of three different Project Mercury development vehicles (see sketches). A dimensionless ratio of internal noise pressure to estimated local dynamic pressure is plotted as a function of Mach number. The upper

two curves are for two Little Joe vehicles, whereas the bottom curve applies to the Big Joe vehicle. The lowest noise pressures measured are for the Big Joe Mercury vehicle. In general, it can be seen that for a given value of local dynamic pressure, the inside noise pressures decrease as the Mach number increases. For the reentry configuration where the blunt base is forward, the aerodynamic noise pressures were noted to be markedly lower than those during the exit phase. The reason for these lower noise pressures in reentry is not fully understood at the present time; however, they are believed to be due in part to the difference in capsule orientation and also to Mach number effects.

Although some minor differences existed in construction and internal sound treatment, it is believed that the differences in the measured noise pressures between Little Joe 2 and the Big Joe vehicle may be ascribed mainly to differences in external geometry. Of particular interest is a direct comparison of the data for Little Joe 2 with that for Little Joe 1B. The resulting internal noise pressures are seen to be markedly higher in this latter case. These noise pressure increases are due possibly to separated flow conditions induced by the spoiler and are of the same order of magnitude as those previously measured in a wind tunnel model having separated flow and different external contours.

SCOUT VEHICLE SURFACE PRESSURE MEASUREMENTS

In conjunction with the launching of an orbital payload for Scout, a so-called "piggy-back" aerodynamic noise experiment was carried out. The nature of this experiment is indicated in figure 23. The vehicle was launched from Wallops Island, Virginia and was tracked by means of a nearby radar facility. The vehicle was instrumented with a telemeter system such that real-time surface pressure fluctuation data were telemetered to a ground receiving station. The experiment was arranged in such a way that usable data were obtained up to the time of second stage ignition. Thus the data included first stage burning, during which time the vehicle passed through the maximum dynamic pressure conditions and achieved a Mach number of about 4, plus the coast period between first stage burnout and second stage ignition.

The test vehicle shape and significant dimensions, along with the on-board equipment, can be described with the aid of figure 24. The vehicle was roughly 72 feet in length with a maximum diameter of 40 inches. The two microphone measuring stations were located approximately 34 feet and 68 feet, respectively, back from the nose. The nature of the on-board measuring and telemetering equipment is indicated by the photographs at the bottom of the figure. The microphones, having a diameter of about 1/2 inch, were flush mounted in the vehicle surface and were connected to an FM telemeter transmitter through the associated amplifier and carrier equipment shown. All of this equipment, with the

exception of the battery power supply and cabling, weighed about 4 pounds.

These instruments, together with ground station tape recording equipment, provided a frequency range of about 20 to 10,000 cps for each microphone channel. Data were obtained for a range of dynamic pressures up to 2300 lbs/sq ft, for Mach numbers up to 4.1, and for Reynolds numbers up to about 400×10^6. It has been estimated, based on incompressible flow considerations, that the boundary-layer thickness was in the range 10 to 20 times the transducer size for the data presented.

Preliminary analysis of the recorded data (ref. 17) has indicated a definite effect of Mach number on the spectral content of the measured pressures, and this is illustrated in figure 25. Data are presented for microphone "A" at two different times in the flight for which the dynamic pressure conditions were essentially equal but the Mach numbers were greatly different. The octave band spectrum for a Mach number of .67 is shown by the circle symbols, and the octave band spectrum obtained at Mach 4.13 is represented by the square symbols. The spectra were noted to have a single broad peak, and this peak moved to higher frequencies as the Mach number increased. In the specific cases illustrated in figure 21, this peak in the spectrum is noted to change from about 2,000 cps at the lower Mach number to about 8,000 cps at the higher Mach number.

The range of surface pressure magnitudes measured during the test

is illustrated in figure 26. It was noted generally that the pressures increased as the dynamic pressure increased, and hence the data are presented in the form of pressure coefficients, $\sqrt{p^{-2}}/q$ where p is the noise pressure and q is the free-stream dynamic pressure. Within the limits shown on figure 26, there seemed to be no marked effect of Mach number over the entire range of the tests from subsonic to supersonic. The dashed portions of the curves at high Mach numbers correspond to flight conditions at high altitudes and very low associated dynamic pressures. The signal-to-noise ratios are rather low at these latter conditions, and thus the dashed curves are based on less reliable data.

The range of pressure coefficient values measured for the Scout tests are compared with similar data from other free flight studies in figure 27. It can be seen that the data compare favorably with those measured for a B-47 and a B-57 airplane as indicated in the figure (see refs. 10 and 11). These values are considerably higher than those measured in reference 12 on the nose cone of a fighter aircraft for which the Reynolds numbers were much lower, and hence the local flow conditions might have been considerably different. The Scout data values are notably lower, however, than those measured in reference 13 for the Mercury spacecraft which had rough external contouring and possible associated flow separation and shock wave interactions. The Scout data are also markedly lower than the localized pressure coefficients measured during buffeting studies of space vehicle models in wind tunnels.

CONCLUDING REMARKS

Discussions were directed to several turbulence sources of boundary-surface fluctuating pressure of aircraft and launch vehicles. It was noted that turbulence is associated with disturbances varying widely in scale and that these are the sources of problems of interior noise, vibration, and unsteady loads. All are significant from the standpoint of satisfactory overall vehicle operation, but each is noted to be important in certain phases of the flight. The opportunity was also taken to present some measurement results of recent studies of atmospheric turbulence and of boundary-layer flows.

REFERENCES

1. Houbolt, John C., Steiner, Roy, and Pratt, Kermit G.: Flight Data and Considerations of the Dynamic Response of Airplanes to Atmospheric Turbulence. Presented to Structures and Materials Panel and to Flight Mechanics Panel, AGARD, Paris, France, July 3-13, 1962.

2. Von Karman, Theodore: Progress in the Statistical Theory of Turbulence. Collected Works of Theodore von Karman, Vol. IV, pp. 362-371, Butterworths Scientific Publications, London, 1940-1951.

3. Boswinkle, Robert W., Jr.: Aerodynamic Problems of Launch Vehicles. NASA SP-11, Proceedings of NASA-Univ. Conf. on the Science and Technology of Space Exploration, Vol. 2, Chicago, Illinois, Nov. 1-3, 1962, pp. 193-201.

4. Garrick, I. E., and Rainey, A. Gerald: Remarks on the State-of-the-Art of Buffet-Loads Prediction. Presented to Structures and Materials Panel, AGARD, Paris, France, July 3-6, 1962.

5. Rainey, A. Gerald, and Runyan, Harry L.: Structural Dynamics Aspects of the Manned Lunar Space Vehicle Launch Phase. Presented at SAE National Aeronautics Meeting, April 3-6, 1962, New York City, SAE Preprint No. 513C.

6. Leech, Frank J., and Sackschewsky, Virgil E.: Boundary Layer Noise Measurements of the F-102 Aircraft. MRL-TDR-62-71, Wright-Patterson Air Force Base, Ohio, August 1962.

7. Mull, Harold R., and Algranti, Joseph S.: Flight Measurement of Wall-Pressure Fluctuations and Boundary-Layer Turbulence. NASA TN D-280, Oct. 1960.

8. McLeod, Norman J.: Flight-Determined Aerodynamic-Noise Environment of an Airplane Nose Cone Up to a Mach Number of 2. NASA TN D-1160, March 1962.

9. Eldred, K., Roberts, William, and White, R.: Structural Vibrations in Space Vehicles. WADD Tech. Rep. 61-62, Wright-Patterson Air Force Base, Ohio, Dec. 1961.

10. McLeod, Norman J., and Jordan, Gareth H.: Preliminary Flight Survey of Fuselage and Boundary-Layer Sound-Pressure Levels. NACA RM H58B11, May 13, 1958.

11. Shattuck, Russell D.: Sound Pressures and Correlations of Noise on the Fuselage of a Jet Aircraft in Flight. NASA TN D-1086, Aug. 1961.

12. Maestrello, Lucio: Boundary Layer Pressure Fluctuations on the 707 Prototype Airplane. Presented at 64'th Meeting, Acous. Soc. Amer., Seattle, Washington, Nov. 7-10, 1962.

13. Mayes, William H., Hilton, David A., and Hardesty, Charles A.: In-Flight Noise Measurements for Three Project Mercury Vehicles. NASA TN D-997, Jan. 1962.

14. Hubbard, Harvey H.: Some Experiments Related to the Noise from Boundary Layers. J. Acous. Soc. Amer., Vol. 29, No. 3, 331-334, March 1957.

15. Rogers, O. R., and Cook, R. F.: Aerodynamic Noise and the Estimation of Noise in Aircraft. WADC Tech. Rept. 52-341, Wright-Patterson Air Force Base, Ohio, Dec. 1952.

16. Willmarth, William W.: Wall Pressure Fluctuations in a Turbulent Boundary Layer. NACA TN 4139, March 1958.

17. Hilton, David A.: Scout Vehicle Aerodynamic Noise Measurements. Paper to be presented at 65'th Meeting, Acous. Soc. Amer., New York City, May 15-18, 1963.

TURBULENCE SOURCES

SOURCE	SIGNIFICANT FREQUENCY RANGE, CPS	SOME EFFECTS
ATMOSPHERIC TURBULENCE GROUND WINDS AND WIND SHEAR	0 – 20	LAUNCH VEHICLE BUFFET WING AND TAIL LOADS (AIRCRAFT) HUMAN BODY VIBRATION, LAUNCH VEHICLE DYNAMIC LOADS, GUIDANCE
BUFFET AND OSCILLATING SHOCKS	1 – 500	MAY EXCITE PRIMARY VIBRATION MODES LOCAL HIGH FREQUENCY RESPONSE
BOUNDARY-LAYER TURBULENCE	100 – 10,000	POSSIBLE HIGH LEVEL PANEL RESPONSE NOISE, SOUND-PROOFING, DISCOMFORT

Figure 1

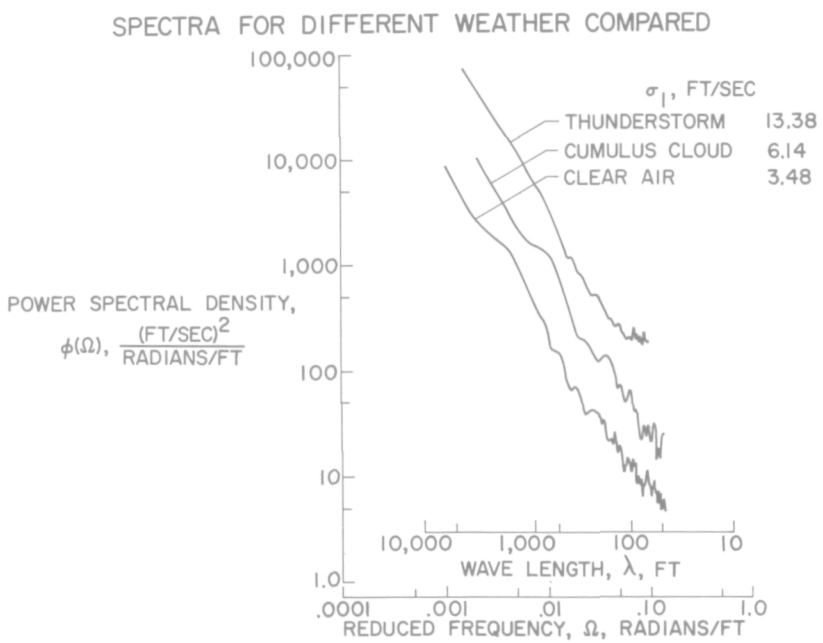

Figure 2

ANALYTICAL REPRESENTATIONS OF POWER SPECTRA AND AUTOCORRELATIONS

CASE I

$$\phi(\Omega) = \frac{\sigma^2 L}{\pi} \qquad \frac{1 + \frac{8}{3}(L_1\Omega)^2}{\left[1 + (L_1\Omega)^2\right]^{11/6}} \qquad (L_1 = 1.339\ L)$$

$$R(r) = \sigma^2\,(0.59253)\left(\frac{r}{L_1}\right)^{1/3}\left[K_{1/3}\left(\frac{r}{L_1}\right) - \frac{1}{2}\,\frac{r}{L_1}\,K_{2/3}\left(\frac{r}{L_1}\right)\right]$$

CASE II

$$\phi(\Omega) = \frac{\sigma^2 L}{\pi} \qquad \frac{1 + 3L^2\Omega^2}{\left[1 + L^2\Omega^2\right]^2}$$

$$R(r) = \sigma^2\left(1 - \frac{1}{2}\,\frac{r}{L}\right)e^{-r/L}$$

Figure 3

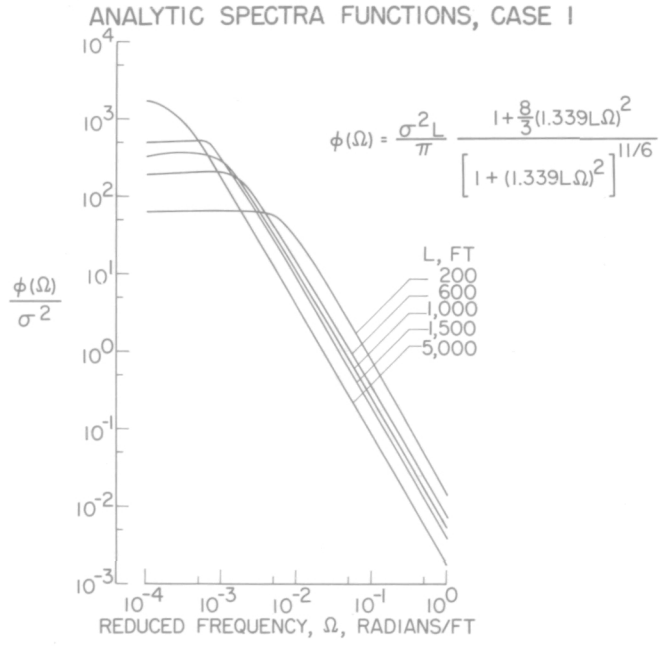

Figure 4

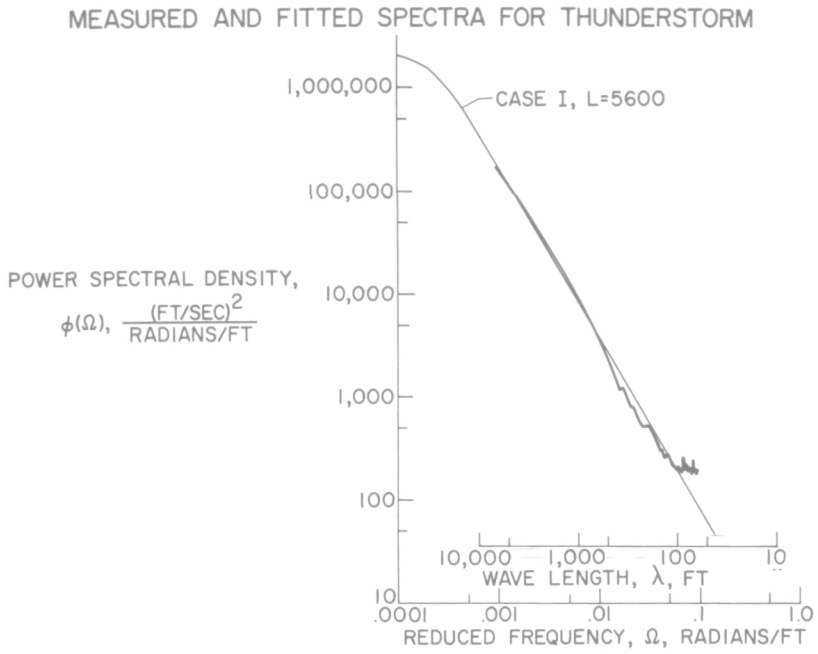

Figure 5

TURBULENCE SCALE, L, FT		
	SPECTRUM	CORRELATION
CASE I	5,550	5,720
CASE II	3,430	4,750

$$L = 2\int_0^\infty \frac{R(r)}{R(0)}\,dr$$

$$R(0) = \sigma^2 = 2\int_0^\infty \phi(\omega)\,d\omega$$

$$\phi(0) = \frac{\sigma^2 L}{\pi}$$

Figure 6

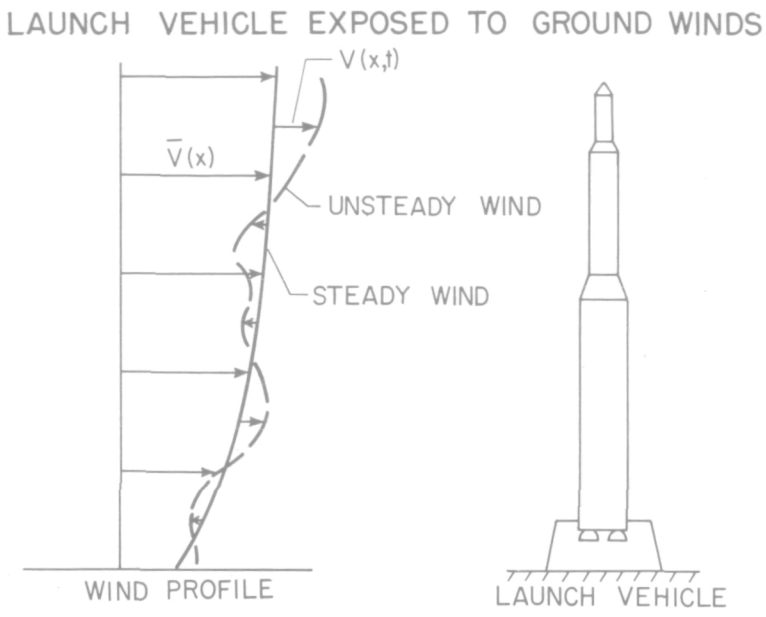

Figure 7

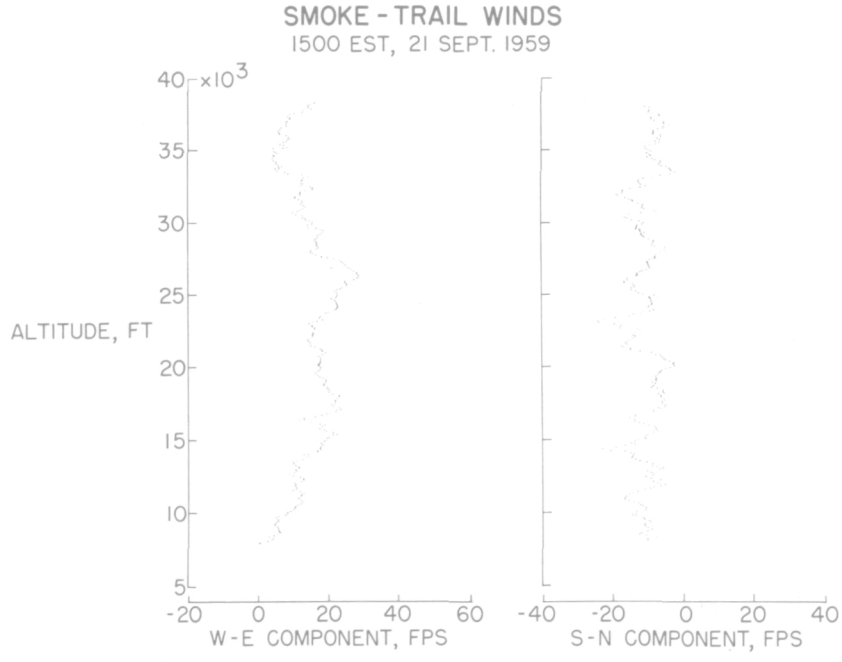

Figure 8

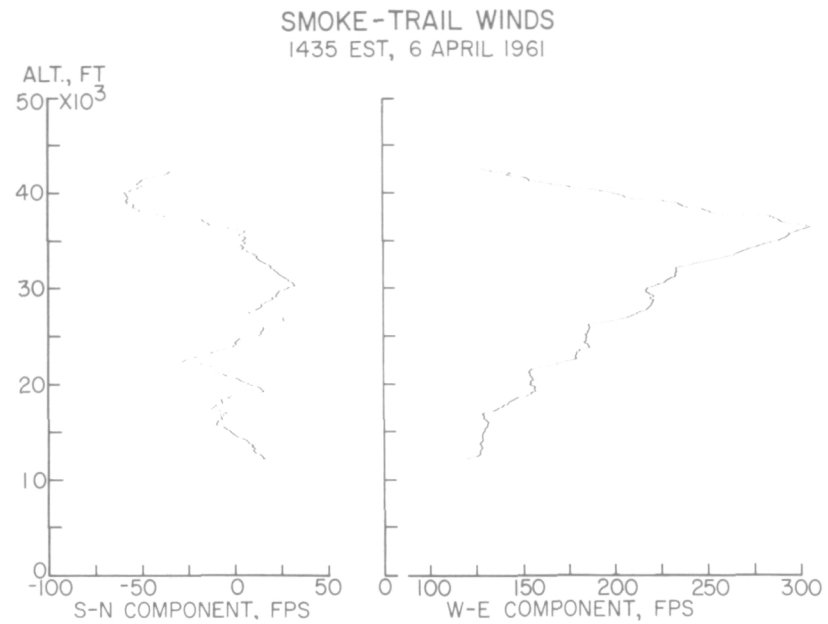

Figure 9

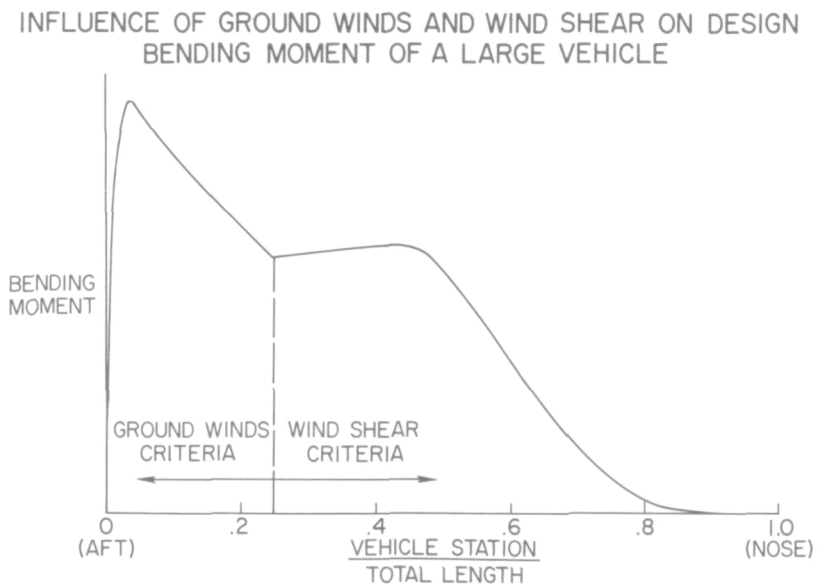

Figure 10

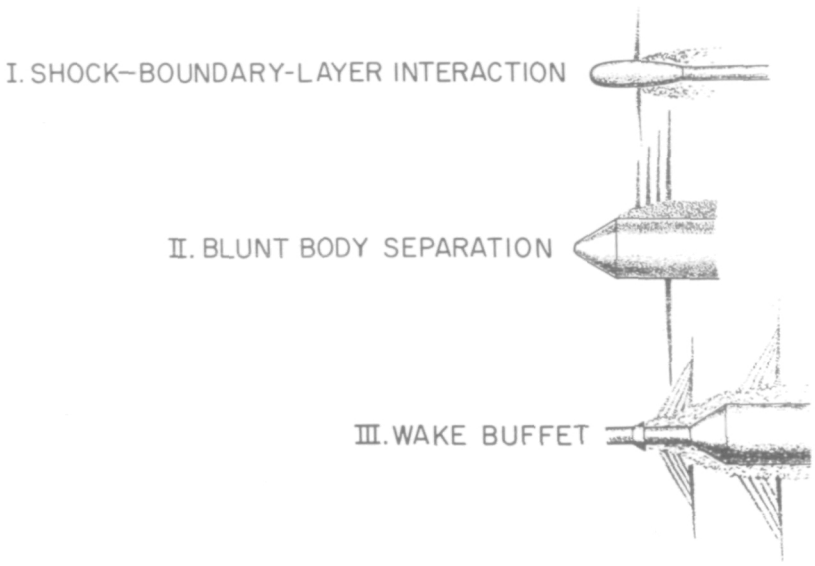

Figure 11

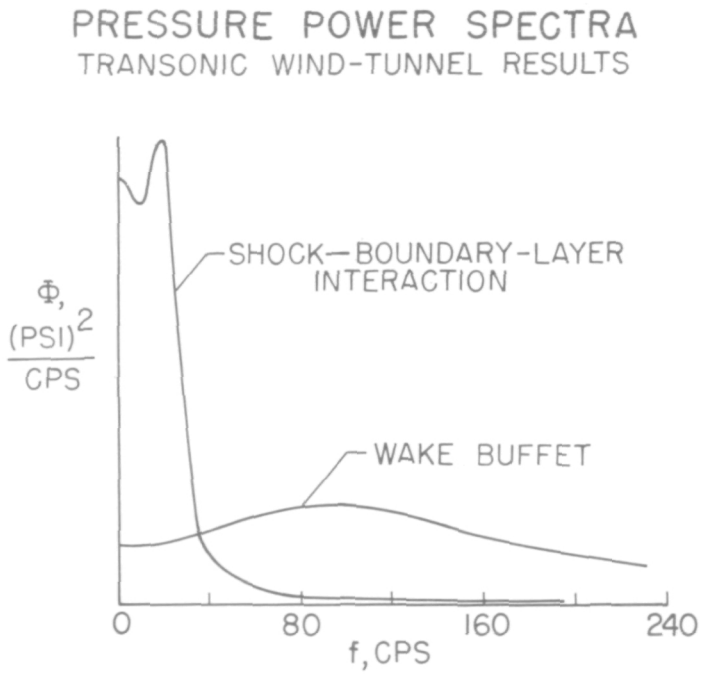

Figure 12

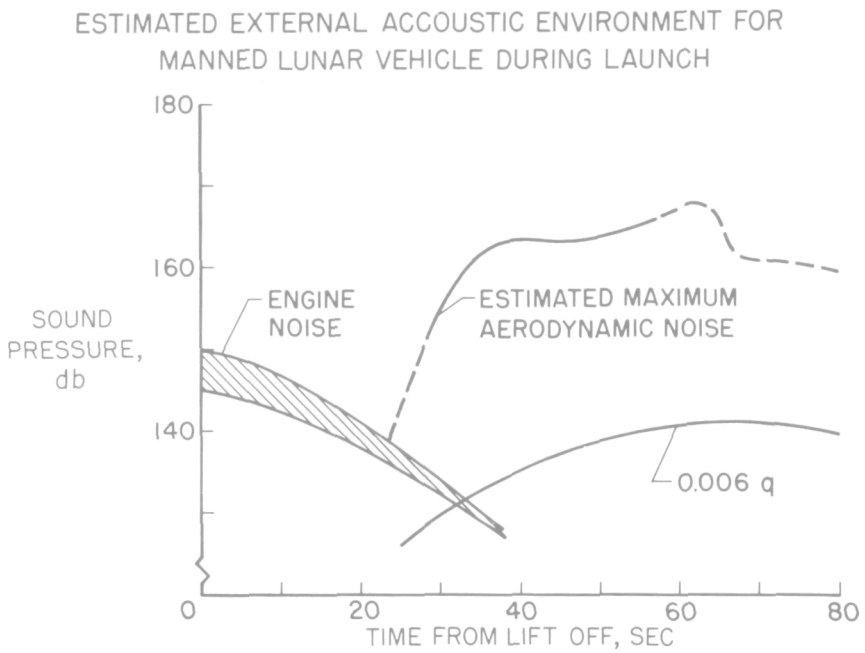

Figure 13

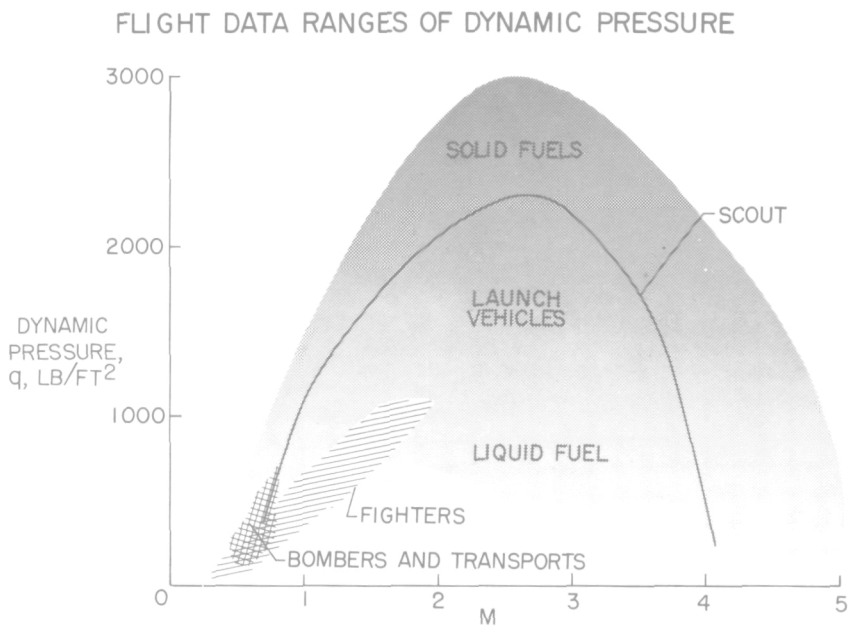

Figure 14

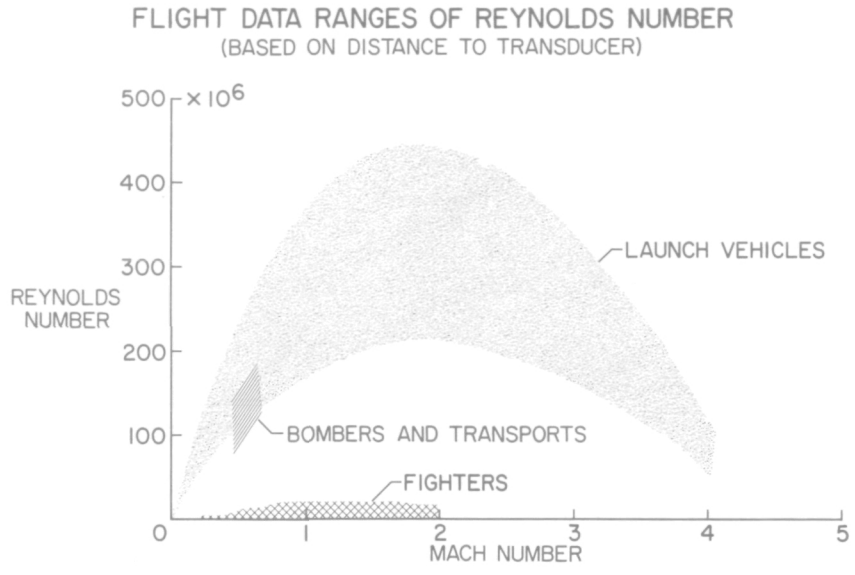

Figure 15

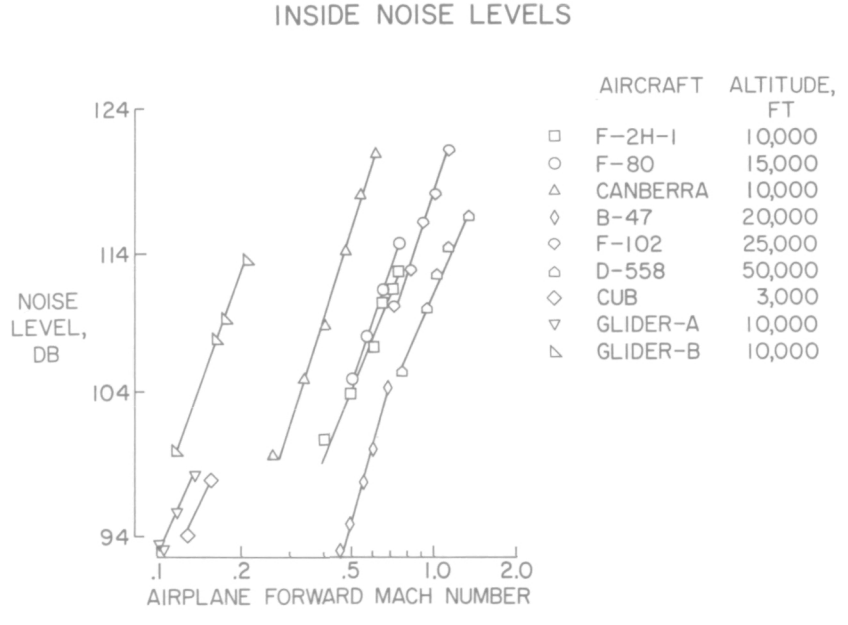

Figure 16

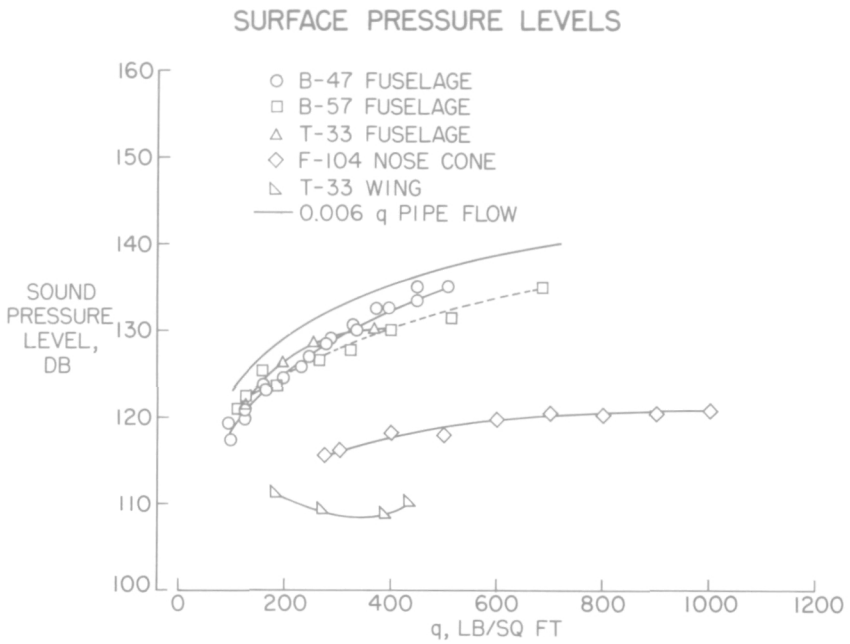

Figure 17

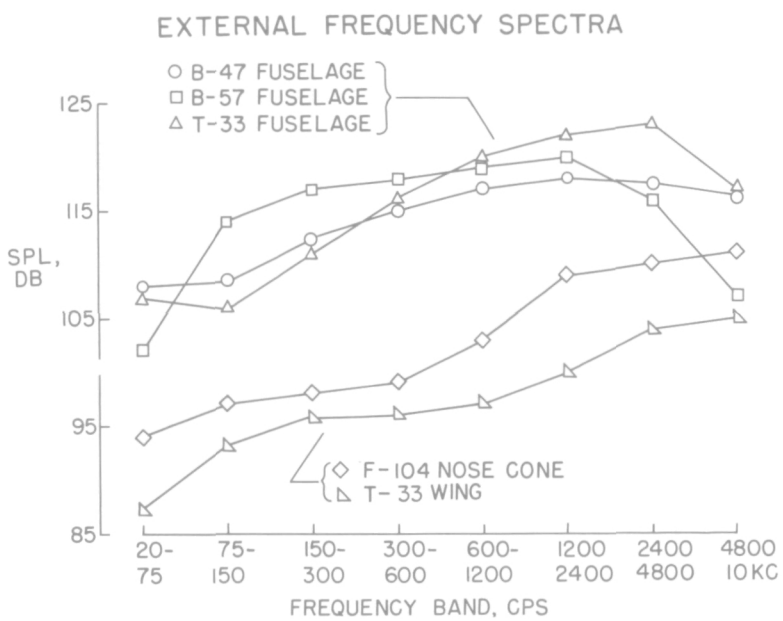

Figure 18

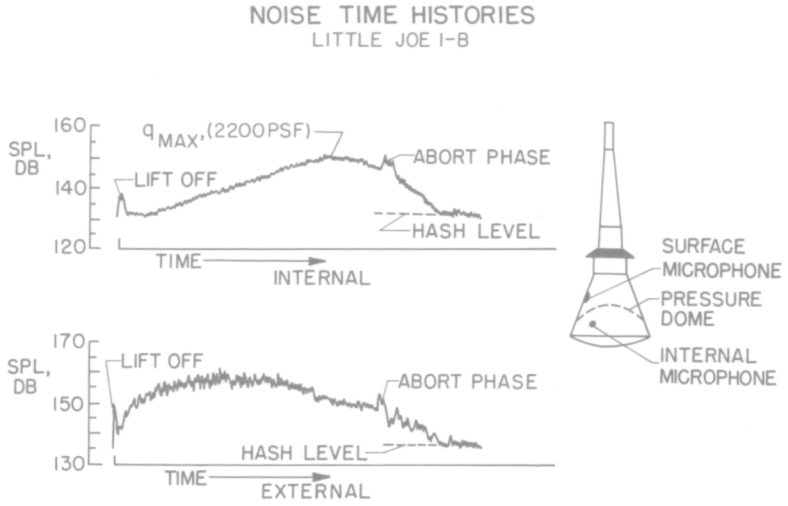

Figure 19

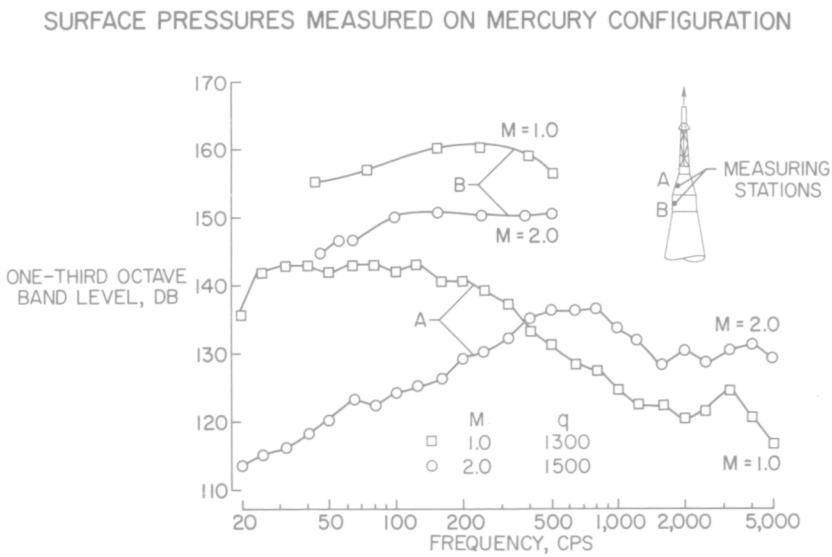

Figure 20

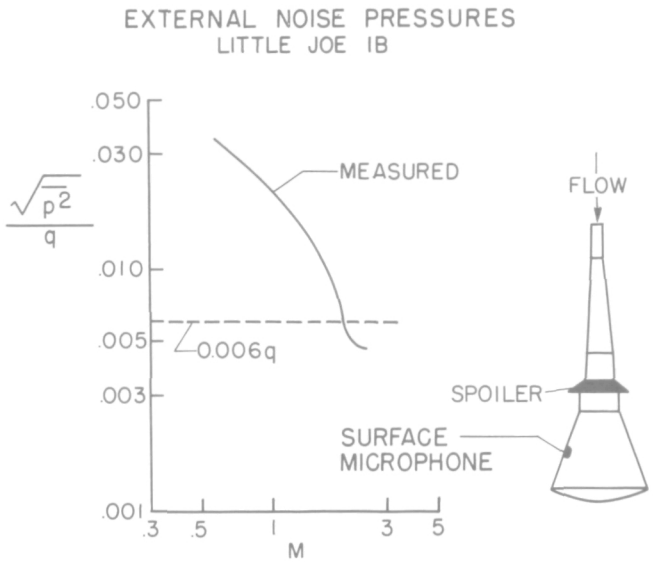

Figure 21

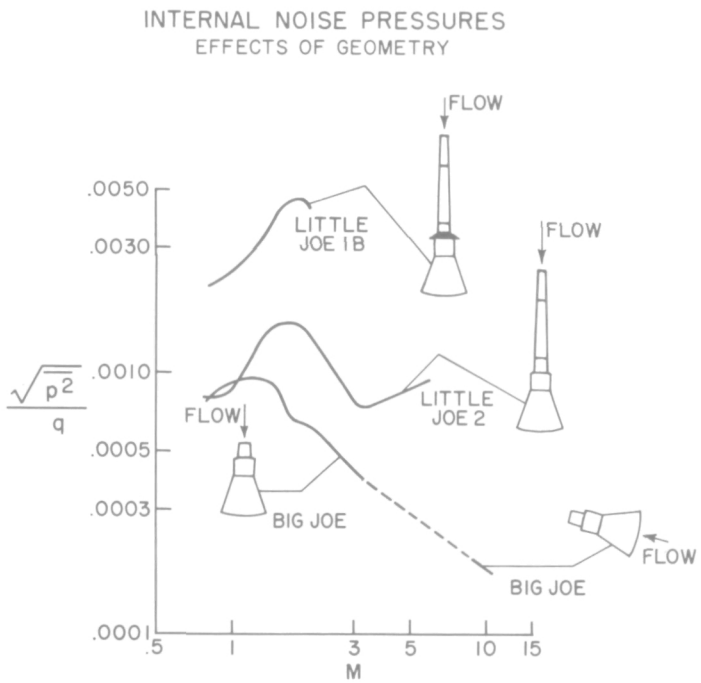

Figure 22

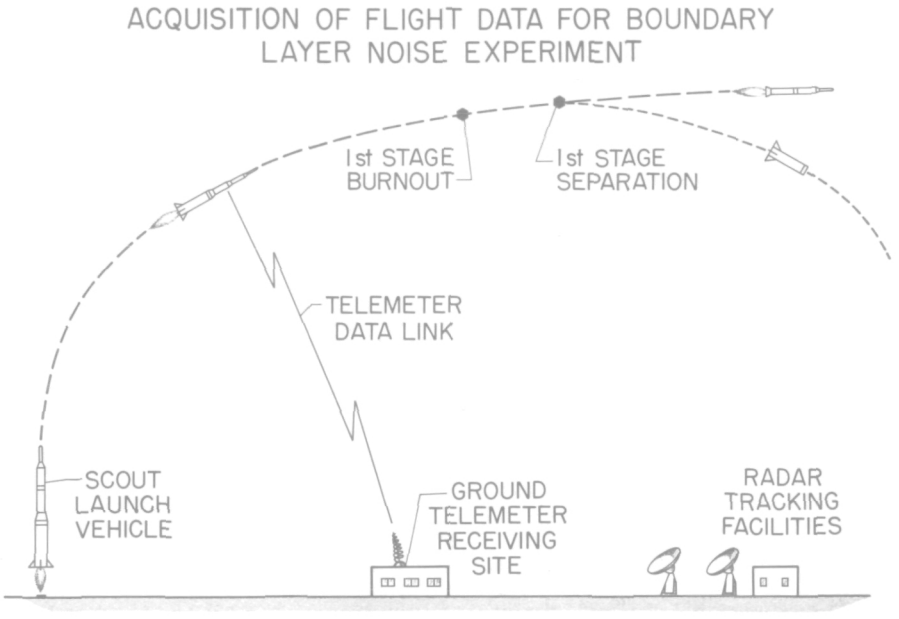

Figure 23

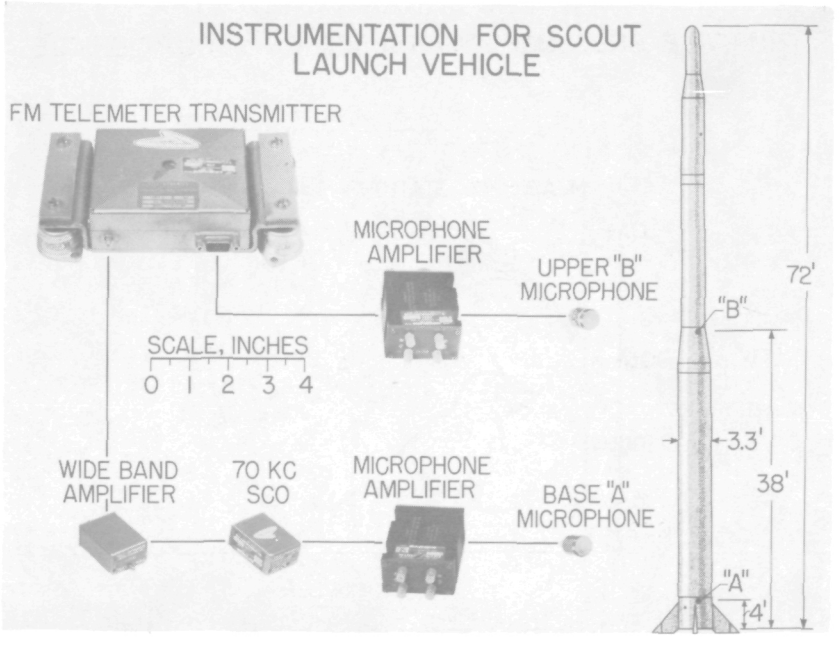

Figure 24

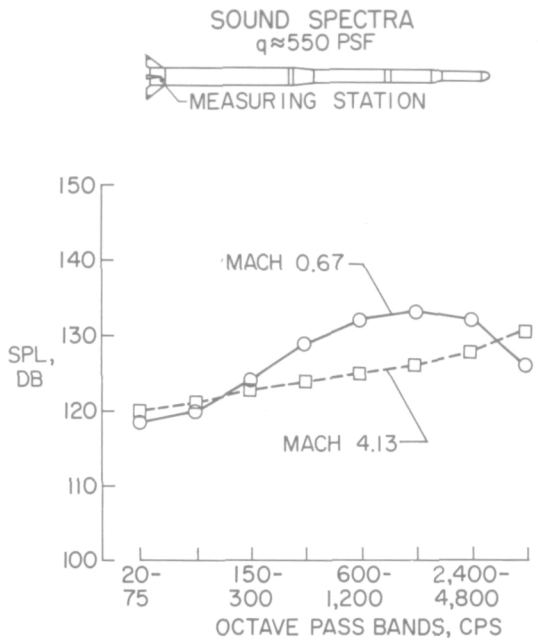

Figure 25

SURFACE PRESSURES MEASURED ON SCOUT VEHICLE

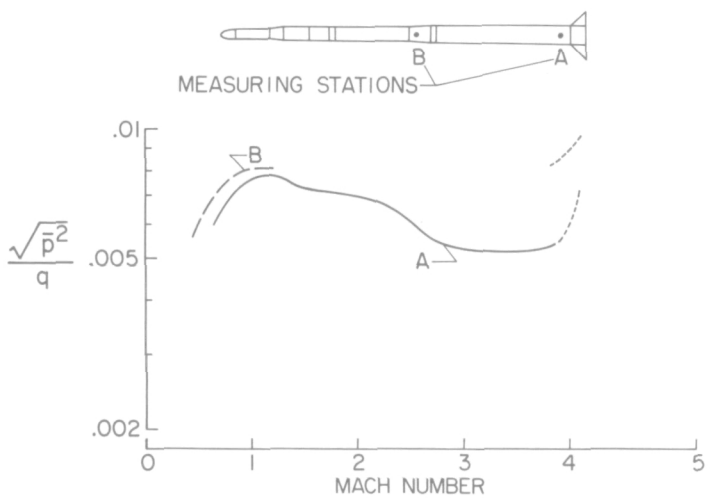

Figure 26

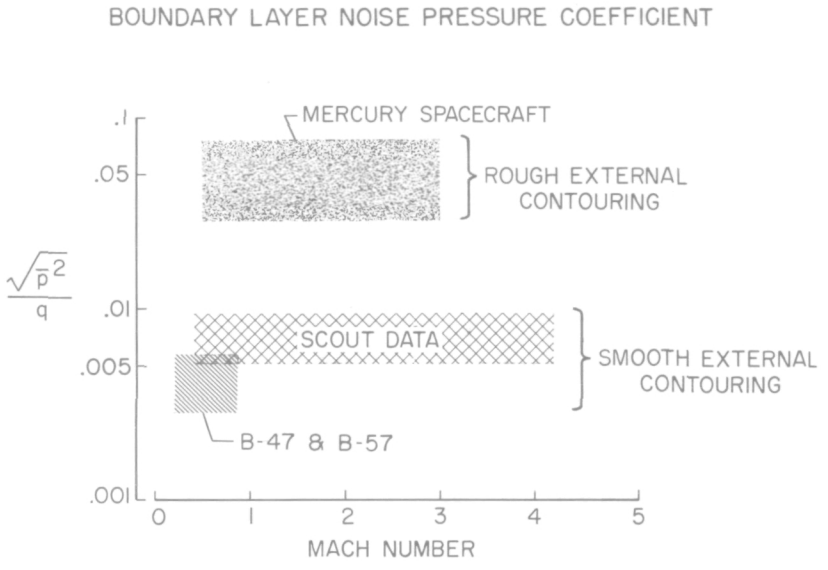

Figure 27

NASA-Langley, 1963